Optics Letters

Fast controllable confocal focus photoacoustic microscopy using a synchronous zoom opto-sono objective

HAIGANG MA,[1,2] ZHONGWEN CHENG,[1] ZHIYANG WANG,[1] KEDI XIONG,[1] AND SIHUA YANG[1,2,*]

[1]*MOE Key Laboratory of Laser Life Science & Institute of Laser Life Science, South China Normal University, Guangzhou 510631, China*
[2]*College of Biophotonics, South China Normal University, Guangzhou 510631, China*
*Corresponding author: yangsh@scnu.edu.cn

Although variable optical focus lenses have been exploited in photoacoustic microscopy (PAM) to improve imaging performance, an optical and acoustic synchronous zoom lens-based confocal PAM system has not yet been achieved previously, to the best of our knowledge. Here we develop a fast controllable confocal focus PAM (FC-PAM) equipped with a synchronous zoom opto-sono objective to facilitate horizontal slice imaging of specimens with irregular surfaces or multilayered structures at different depths. The integration of an opto-sono objective of an electrowetting-based zoom lens allows for the adjustment of the confocal focal length. Using this objective, the FC-PAM achieved a confocal focus-shifting range of approximately 6 to 43 millimeters with a high transverse resolution, and the confocal focus-shifting time was substantially reduced. Phantom experiments and human skin imaging were performed to demonstrate that the opto-sono objective has great potential for studying living biological tissue and promoting the development of *in vivo* rapid-noninvasive PAM depth imaging.   © 2019 Optical Society of America

https://doi.org/10.1364/OL.44.001880

Photoacoustic microscopy (PAM) combines the advantages of rich optical absorption contrast and weak ultrasonic scattering in tissue [1–3]. In most PAM systems, synchronous axial scanning of the transducer and optical lens is required owing to the degradation of resolution and sensitivity in the region outside of the acoustic and optical focus [4,5]. This is particularly relevant in the case of horizontal slice imaging of specimens that range from several millimeters to several centimeters with irregular surfaces or multilayered structures. However, due to the single depth of focus in most PAM implementations, only a narrow depth range is acquired in focus. Mechanical scanning mode can be used to improve the depth of field by moving the photoacoustic (PA) objective or sample with a motor-driven linear platform in the depth direction; however, the synchronous axial scanning of the detector and the optical lens is difficult to achieve and the focus-shifting speed is limited by the

mechanical inertia of the moving components [6,7]. In order to achieve fast focus-shifting, tunable lenses have been exploited and previously reported in PAM [8–10]. In such cases, the limitation of the system is that only a single mode of the optical or acoustic axial scanning is typically implemented, which cannot satisfy the requirement of a wide range of depth focusing. Thus, in this report, an optical resolution fast controllable confocal focus PAM (FC-PAM) using a synchronous zoom opto-sono objective has been developed, which facilitates optical and acoustic synchronous focusing scanning over a wide depth range. The opto-sono objective is composed of an electrowetting-based zoom lens and a polyvinylidene fluoride (PVDF) transducer. The electrowetting-based lens made out of two immiscible transparent liquids that are used as optical-acoustic lenses, represents an application of the electrowetting effect: changes of the wetting properties of a liquid on a solid induces changes in the radius of curvature of the liquid-liquid interface by modifying the applied voltage at the solid-liquid interface, which then changes the resulting focal length [11,12]. If the optical and acoustic beams can pass through the liquid-liquid interface with the same refractive index of the zoom lens, it is possible to realize a coaxial confocal configuration of optical illumination and acoustic detection, so that the confocal focal lengths of the FC-PAM system can be varied as a function of the supplied electrical signal and continuously adjusted. The opto-sono objective has several advantages, including the following: (1) it can synchronously shift the optical and acoustic focuses in the depth direction and simultaneously maintain a coaxial confocal configuration of optical illumination and acoustic detection, which greatly reduces the focus-shifting time; (2) it can satisfy the requirement of a wide range of depth focusing with high resolution and sensitivity for horizontal slice imaging of specimens with irregular surfaces or multilayered structures at different depths; (3) the PVDF element has an inherent low acoustic impedance that matches well with *in vivo* tissue, and has the advantages of high sensitivity and a wide bandwidth for PA imaging [13]. The performance of the FC-PAM system has been evaluated in phantom and human skin experiments.

Similar to most PAM imaging systems, as shown in Fig. 1(a), the visible laser beam (532 nm) generated by a
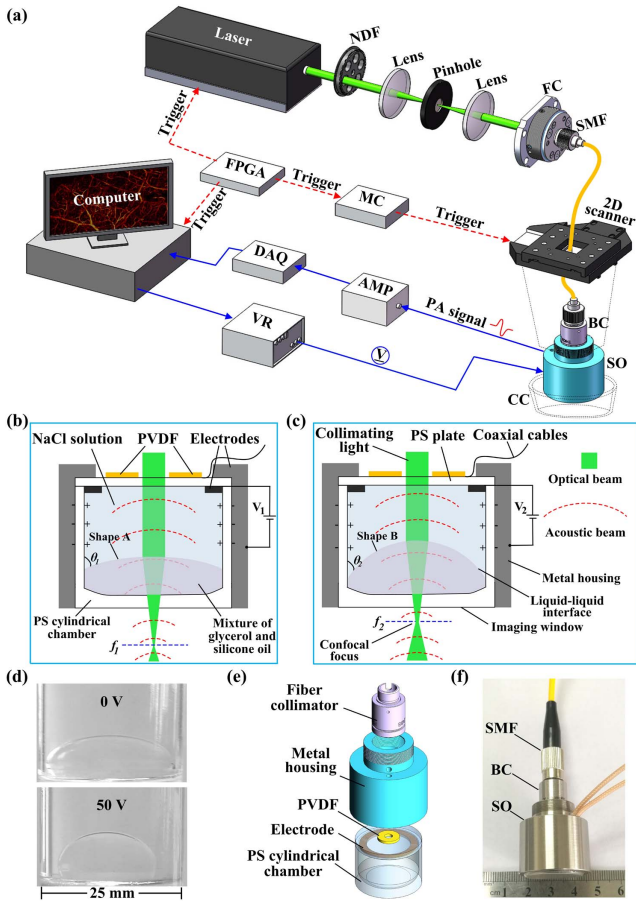
Fig. 1. Design and operating principle of FC-PAM. (a) Schematic of the FC-PAM imaging system. NDF, neutral-density filters; FC, fiber coupler; SMF, single-mode fiber; BC, beam collimator; MC, motor driver; DAQ, data acquisition card; AMP, amplifier; VR, voltage regulator; SO, synchronous zoom opto-sono objective; CC, coupling cup. (b)–(c) Schematic cross-section of the opto-sono objective in a cylindrical housing, not to scale. PVDF, polyvinylidene fluoride; PS, polystyrene. (d) Photograph of a 25 mm diameter electrowetting lens without voltage (0 V) and an applied voltage (50 V). (e) Perspective view of components prior to assembly, showing the fiber collimator, metal housing, and core part of the lens. (f) Image of the opto-sono objective.

Q-switched pulsed laser (DTL-314QT, Laser-export) first passes through a spatial filter, then is coupled into a single-mode fiber using a fiber coupler (PAF-X-7-A, Thorlabs). The entire imaging probe consists of a beam collimator (F240FC-532, Thorlabs), a synchronous zoom opto-sono objective, and a two-dimensional scanner that was used to actuate the objective. A transparent coupling cup was placed under the objective for optical and acoustic penetration, which was filled with 10 ml of deionized water and enabled acoustic coupling between the test and detection surfaces of the objective. The PA signals captured were amplified (LNA-650, RFBAY), digitalized (M3i.4110, Germany), and stored in a computer. Figures 1(b) and 1(c) are schematic representations of the principle of operation of the opto-sono objective. Two immiscible liquids, one conducting a NaCl solution and the other an insulating mixture of glycerol and silicone oil are confined

in the polystyrene (PS) cylindrical chamber. The two liquids are transparent with refractive indices that can realize a coaxial confocal configuration of optical illumination and acoustic detection, but with approximately the same density, such that gravity does not deform the liquid-liquid interface, which remains spherical regardless of the orientation of the metal housing. The mixture of glycerol and silicone oil has the shape of a liquid drop in contact with a thin insulating PS material window. The window's surface is hydrophobic, so that the mixture of glycerol and silicone oil will naturally sit on top of it. The metal housing is coated with an electrode followed by an insulating and a hydrophobic coating. In addition, the lower surface of the transparent sealing PS plate is covered with a ring-shaped electrode which is insulated from the electrode of the metal housing. The piezoelectric element of the 25 MHz ring-shaped transducer is made of PVDF material. The thickness of the PVDF element is 20 μm, and the diameter of the working is 6 mm, with a 1.5 mm center aperture for the exit of the laser beam. The PVDF element is coated with silver electrodes at both sides, and then attached to the upper surface of the PS plate with epoxy resin. Based on the above customization, the liquid-liquid interface of the objective can change from shape A to shape B by modifying the applied voltage (V_1 to V_2), so that the confocal focal length (f_1 to f_2) of the optical and acoustic beams is changed. Figure 1(d) shows two images of the objective in two switching states, demonstrating the principle of operation of the objective. The perspective views of components prior to assembly and imaging of the objective are shown in Figs. 1(e) and 1(f). According to the principle of electrowetting [11,12], if the refractive index of the NaCl solution is different from that of the mixture of glycerol and silicone oil, the objective system can be considered as a variable focus lens. Equation (1) describes how the applied voltage U changes the radius of the interface r [14]:

$$r = -a/[\cos\theta_0 + \varepsilon_0\varepsilon_r U^2/(2\gamma d)], \tag{1}$$

where a is the inner radius of PS cylindrical chamber, θ_0 is the natural contact angle at zero voltage, ε_0 is the permittivity of free space and ε_r is the relative permittivity, γ is the tension coefficient of the liquid-liquid interface, and d is the thickness of sidewalls of PS cylindrical chamber. Meanwhile, the optical and acoustic relative refractive indices can be calculated by the following equations:

$$n_{\text{optic}} = n_{\text{NaCl}}/n_{\text{oil}}, \tag{2}$$

$$n_{\text{acoustic}} = v_{\text{oil}}/v_{\text{NaCl}}, \tag{3}$$

where n_{NaCl} and n_{oil} represent, respectively, the optical refractive indices of the NaCl solution and mixture of glycerol and silicone oil, and v_{NaCl} and v_{oil}, respectively, are the sound velocities of the NaCl solution and mixture of glycerol and silicone oil. A coaxial confocal configuration with optical illumination and acoustic detection is possible if the NaCl solution has a lower refractive index and a higher sound velocity compared with the mixture of glycerol and silicone oil [2]. We note that the 22% NaCl solution with a high optical refractive index (1.37) and a modest sound velocity (1711 mm/μs) serves well as the conducting solution. By the known NaCl solution and mentioned formulas, we purposely chose a glycerol (57%) and silicone oil (43%) mixture as the insulating liquid [2,10]. The mixture had an optical refractive index of 1.46, and the

speed of sound in this mixture was 1605 mm/µs. The acoustic impedance of this mixture was 2.54 MRayl [15,16]. The densities of both the 22% NaCl solution and the mixture of glycerol and silicone oil are approximately $1.145 g/\text{cm}^3$. Hence, it is feasible to achieve acoustic and optical confocal focus by using ~0.85 ml of 22% NaCl solution as the conducting solution and ~0.15 ml of a mixture of glycerol and silicone oil as the insulating liquid.

For FC-PAM, the field characteristic of the opto-sono objective is a key factor that determines the accuracy of image reconstruction. To capture an optical spot, a phantom was made of the transparent gelatin, which was used as a background for optical transmission. The optical intensity distributions were recorded with a CCD camera. To test the acoustic characteristics of the built opto-sono objective shown in Fig. 1, the objective was driven by a pulser/receiver (5073PR, Olympus) to emit ultrasound pulses. A hydrophone (HPM02, Precision Acoustics Ltd.) was used to scan axially and laterally while detecting the ultrasound pulses from the objective by a scanning step of ~20 µm. Figures 2(a) and 2(b) show the optical rays and acoustic pressure distributions when two different voltages of 40 and 50 V are applied. It is seen that the opto-sono objective enables a coaxial acoustic and optical confocal configuration with focal lengths of 11 and 8 mm, respectively. The confocal length of the objective was controlled by a custom-built high-precision voltage regulator, which delivered a stable voltage output from 0 to 60 V, with a resolution of 10 mV. Within the control voltage range, the maximum confocal focus-shifting range was measured at approximately 37 mm with a ~10 µm continuously shifting accuracy, as shown in Fig. 2(c). Figure 2(d) shows the pulse response of the detector at the focus (black line), and the blue dotted line is the corresponding Hilbert-transformed envelope. The axial resolution can be taken as the full width at half-maximum of the envelope, which is measured to be ~58 µm.

In the FC-PAM, we used a laser with a repetition rate of 1 KHz, so the image uniform acquisition time is approximately 2 s for a ~5 mm B-Scan PA imaging area with a scanning step of ~5 µm, and the response time of the opto-sono objective is ~50 ms. In order to avoid the influence of the inertia of the liquids, we eliminated the acceleration and deceleration processes of the opto-sono objective during PA imaging. Lateral and axial resolution experiments were performed to verify the imaging capability of the opto-sono objective when different voltages were applied. A surgical blade was put into the sink shown in Fig. 3(a) and experimentally quantified by imaging this object as indicated in Fig. 3(b), with a scanning step of ~2 µm. The lateral resolutions were estimated to be 28 and 13 µm for the application of 40 and 50 V, respectively, as shown in Fig. 3(c). In order to measure the actual axial resolution, transparent agar pieces were prepared and two carbon rods (50 µm diameter) were inserted at different depths (the separation distance was approximately 2.5 mm) of the phantom, as shown in Fig. 3(d). Figure 3(e) showed the reconstructed images of the PA tomography when 40 and 50 V were applied, respectively. The tangential profiles of the images (40 and 50 V) are plotted in Figs. 3(f) and 3(g). In addition, the axial resolution was estimated to be 74 and 62 µm, respectively. The comparison indicates that the objective can efficiently suppress the deformation by enlarging the acceptance angle of the transducer.

To demonstrate the feasibility of the opto-sono objective on biological tissues, the focusing scan imaging of the FC-PAM system and a variable optical focus PAM (VO-PAM) system were compared. The main difference between the VO-PAM and FC-PAM was the addition of a variable optical focus lens (Arctic 25H, Varioptic) between the beam collimator and the
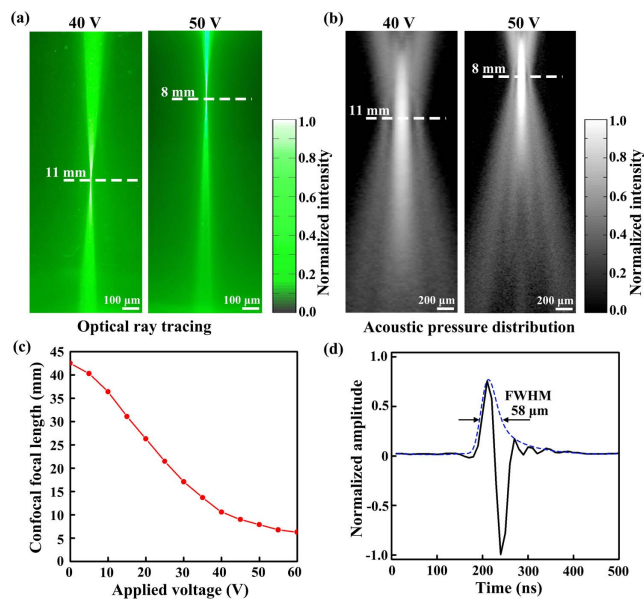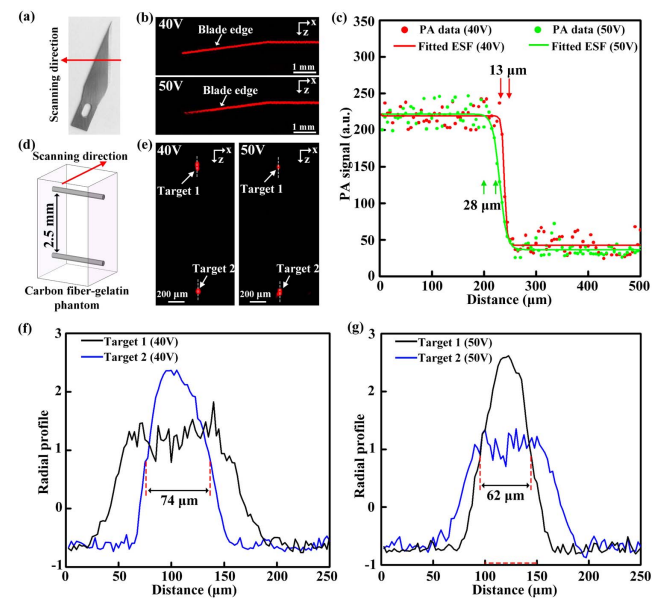
Fig. 2. Optical and acoustic characteristics of the opto-sono objective. (a)–(b) Optical rays and acoustic pressure distribution when voltages of 40 and 50 V are applied. (c) Confocal focal length variation of applied voltage. (d) Pulse response of the transducer at the focus.

Fig. 3. Resolution of the FC-PAM system when voltages of 40 and 50 V are applied. (a) Photo showing the blade target and scanning direction. (b) B-scan PA images of the blade in the focal plane. (c) 1D profile horizontally along one surgical blade is shown in (a). ESF, edge-spread function. (d) 3D schematic rendering of the phantom imaging experiment. (e) Axial section PA images of two carbon fibers. (f)-(g) Axial profile of the carbon fibers in (e).
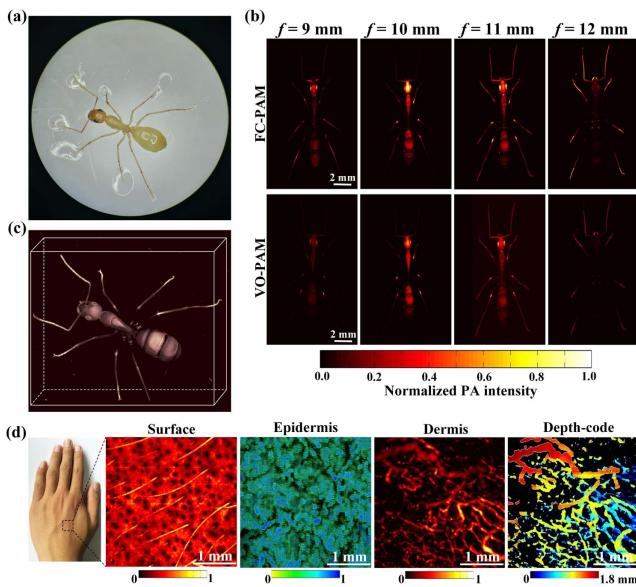
Fig. 4. Focusing scan imaging of the FC-PAM system. (a) Photo image of a camponotus turcestanus. (b) PA images of the camponotus turcestanus, respectively, were acquired using the FC-PAM system and the variable optical focal length PAM system (VO-PAM) at different focal lengths. (c) 3D PA image of the camponotus turcestanus acquired using the FC-PAM system. (d) Horizontal slice imaging of the opisthenar skin by the FC-PAM system at different focusing depths (skin surface, epidermis, and dermal vascular from left to right; the focal length interval was ~0.5 mm between PA images.).

built opto-sono objective, which ensures the consistency of the optical illumination and acoustic detection of the two systems. The objective maintained a constant applied voltage of 40 V in the VO-PAM for imaging, i.e., the acoustic focus was not changed, and focusing scan imaging was performed by only adjusting the variable optical focus lens. Figure 4(a) showed a schematic illustration of the camponotus turcestanus experiment. The camponotus turcestanus was fixed in the sink, and the upper part was close to the objective, while the lower part is farther away from the objective. A total of 2000 A-lines was collected from a B-scan with focal lengths of 9, 10, 11, and 12 mm, separately, and 1600 B-scans, to recover a volume rendered image. All camponotus turcestanus images were generated using PA signals collected over 10×16 mm^2 (scan points, 2000×1600), with an acquisition time of ~1.9 h per PA image. In Fig. 4(b), focusing scan PA images of the camponotus turcestanus were obtained using the FC-PAM and VO-PAM systems. Evidently, the FC-PAM can achieve higher sensitivity imaging compared with the VO-PAM over a wide range of depth focusing scan. A 3D pseudocolor visualization of the camponotus turcestanus is shown in Fig. 4(c) for an applied voltage of 45 V. The horizontal slice imaging of opisthenar skin from one of the authors was performed using the FC-PAM for different confocal lengths, as shown in Fig. 4(d). All human skin images were generated using PA signals

collected over 3×3 mm^2 (scan points, 600×300), with an acquisition time of ~8.5 min per PA image. The imaging results show that the FC-PAM could clearly display the multi-layered structure of skin (skin surface, epidermis, and dermis). To conform to the American National Standards Institute safety limit [17], the laser pulse energy on the skin surface was limited to 80 nJ.

In summary, we developed an optical resolution FC-PAM using an opto-sono objective that allows for a relatively high sensitivity and works well for phantom and *in vivo* imaging. The FC-PAM, which has the advantage of electronically controlled confocal focal length adjustment, can effectively address the issues of transverse resolution and image contrast deterioration, as the focus is moved away from the target. As such, that has the potential for future biomedical applications. It should be noted that the synchronous zoom opto-sono objective facilitates the acquisition of high resolution 3D imaging of specimens with irregular surfaces using the proposed automatic focusing technology. To reduce the impact of acceleration and deceleration processes of the 2D scanner during PA imaging, the use of smaller volumes of the liquids is an important next step in the development of the FC-PAM system.

REFERENCES

1. L. V. Wang and S. Hu, Science **335**, 1458 (2012).
2. L. Xi, C. Song, and H. Jiang, Opt. Lett. **39**, 3328 (2014).
3. H. Ma, S. Yang, Z. Cheng, and D. Xing, Opt. Lett. **42**, 2342 (2017).
4. F. Gao, X. Feng, Y. J. Zheng, and C. D. Ohl, J. Biomed. Opt. **19**, 067006 (2014).
5. Z. Xie, S. Jiao, H. F. Zhang, and C. A. Puliafito, Opt. Lett. **34**, 1771 (2009).
6. W. Göbel and F. Helmchen, J. Neurophysiol. **98**, 3770 (2007).
7. M. Nasiriavanaki, J. Xia, H. L. Wan, A. Q. Bauer, J. P. Culver, and L. V. Wang, Proc. Natl. Acad. Sci. USA **111**, 21 (2014).
8. B. Li, H. Qin, S. Yang, and D. Xing, Opt. Express **22**, 20130 (2014).
9. P. Hajireza, A. Forbrich, and R. J. Zemp, Opt. Lett. **38**, 2711 (2013).
10. C. Song, L. Xi, and H. Jiang, Opt. Lett. **38**, 2930 (2013).
11. F. Mugele and J.-C. Baret, J. Phys. Condens. Matter **17**, R705 (2005).
12. B. Bergea and J. Peseux, Eur. Phys. J. E. **3**, 159 (2000).
13. G. Feng and G. Chu, Sens. Actuators A, Phys. **208**, 130 (2014).
14. R. Peng, J. Chen, C. Zhu, and S. Zhuang, Opt. Express **15**, 6664 (2007).
15. C. Li, G. Ku, and L. V. Wang, Phys. Rev. E **78**, 021901 (2008).
16. J. J. Niederhauser, M. Jaeger, and M. Frenz, Appl. Phys. Lett. **85**, 846 (2004).
17. Laser Institute of America, American National Standard for Safe Use of Lasers ANSI Z136.1-2014.